

Fermi National Accelerator Laboratory

FERMILAB-Conf-96/353

Electroweak Results from the Tevatron

M. Demarteau

*Fermi National Accelerator Laboratory
P.O. Box 500, Batavia, Illinois 60510*

October 1996

Invited talk at *The Workshop on New Directions for High Energy Physics (Snowmass '96)*, Snowmass, Colorado, June 25-July 12, 1996.

Disclaimer

This report was prepared as an account of work sponsored by an agency of the United States Government. Neither the United States Government nor any agency thereof, nor any of their employees, makes any warranty, express or implied, or assumes any legal liability or responsibility for the accuracy, completeness or usefulness of any information, apparatus, product or process disclosed, or represents that its use would not infringe privately owned rights. Reference herein to any specific commercial product, process or service by trade name, trademark, manufacturer or otherwise, does not necessarily constitute or imply its endorsement, recommendation or favoring by the United States Government or any agency thereof. The views and opinions of authors expressed herein do not necessarily state or reflect those of the United States Government or any agency thereof.

Distribution

Approved for public release: further dissemination unlimited.

Electroweak Physics Results from the Tevatron *

Marcel Demarteau
Fermi National Accelerator Laboratory
P.O. Box 500, Batavia, IL 60565

ABSTRACT

An overview of recent electroweak physics results from the Tevatron is given. Properties of the W^\pm and Z^0 gauge bosons using final states containing electrons and muons based on large integrated luminosities are presented. In particular, measurements of the W^\pm and Z^0 production cross sections, the W -charge asymmetry and the measurement of the W -mass are summarized. Gauge boson self interactions are measured by studying gauge boson pair production and limits on anomalous gauge boson couplings are discussed.

I. INTRODUCTION

The Standard Model of electroweak interactions (SM) has taken a very prominent position in today's description of experimental results. Perhaps the most compelling reason for this state of affairs is that the experimental results have reached a level of precision which require a comparison with theory beyond the Born calculations, which the SM is able to provide. It is widely anticipated, though, that the SM is just an approximate theory and should eventually be replaced by a more complete and fundamental description of the underlying forces in nature. Since the highest center of mass energies are reached at the Tevatron, the measurements at this accelerator provide natural tools to probe the SM at the highest energy scale.

In this summary the most recent electroweak results from the Tevatron will be described, with the emphasis on results from the collider experiments CDF and DØ. The CDF and DØ detectors are large multi-purpose detectors operating at the Fermilab Tevatron $\bar{p}p$ Collider [1, 2]. The DØ detector has a non-magnetic inner tracking system, compact, hermetic, uranium liquid-argon calorimetry and an extensive muon system. The CDF detector has a magnetic central detector, scintillator based calorimetry and a central muon system. During the 1992-1993 run, generally called Run 1a, the CDF and DØ experiments have collected $\sim 20 \text{ pb}^{-1}$ and $\sim 15 \text{ pb}^{-1}$ of data, respectively. For the 1994-1995 run (Run 1b) both experiments have collected $\sim 90 \text{ pb}^{-1}$ of data. The CCFR experiment at Fermilab studies ν_μ -nucleon interactions. The measurement of the ratio of charged and neutral current cross sections provides a direct measurement of the weak mixing angle. Results on the W and Z production cross sections, the W -width, W -charge asymmetry and the mass of the W -boson are presented. In the last section moments of the gauge boson are discussed.

II. IVB PRODUCTION CROSS SECTIONS

In $\bar{p}p$ collisions intermediate vector bosons are produced predominantly by quark-antiquark annihilation. In approximately 80% of the interactions a valence quark is involved. Sea-sea interactions contribute $\approx 20\%$ to the total cross section. The leptonic decay modes of the W and Z -bosons are easily detected because of their characteristic decay signatures: for a W decay a high p_T lepton accompanied by large missing transverse energy (E_T), indicating the presence of a neutrino, and two high p_T leptons for Z -decays. The measurement of the W and Z production cross sections probes the SM of electroweak and strong interactions and provides insight in the structure of the proton. With the large increase in integrated luminosity the new measurements have a significantly improved precision. A persistent uncertainty on any cross section measurement at a $\bar{p}p$ collider, however, is the large uncertainty on the integrated luminosity due to the uncertainty on the effective total $\bar{p}p$ cross section seen by the detectors. This uncertainty cancels completely in the ratio of the W and Z production cross sections, a quantity that can be used to extract the width of the W -boson, $\Gamma(W)$. The event selection is thus geared towards maximizing the cancellation of the different uncertainties in the ratio of the two cross section measurements.

	DØ		CDF	
	e	μ	e	μ
W cand.	59579	4472	13796	6222
A_W (%)	43.4 ± 1.5	20.1 ± 0.7	34.2 ± 0.8	16.3 ± 0.4
ϵ_W (%)	70.0 ± 1.2	24.7 ± 1.5	72.0 ± 1.1	74.2 ± 2.7
Bkg (%)	8.1 ± 0.9	18.6 ± 2.0	14.1 ± 1.3	15.1 ± 2.2
$\int \mathcal{L} \text{ (pb}^{-1}\text{)}$	75.9 ± 6.4	32.0 ± 2.7	19.7 ± 0.7	18.0 ± 0.7
Z cand.	5702	173	1312	423
A_Z (%)	34.2 ± 0.5	5.7 ± 0.5	40.9 ± 0.5	15.9 ± 0.3
ϵ_Z (%)	75.9 ± 1.2	43.2 ± 3.0	69.6 ± 1.7	74.7 ± 2.7
Bkg (%)	4.8 ± 0.5	8.0 ± 2.1	1.6 ± 0.7	0.4 ± 0.2
$\int \mathcal{L} \text{ (pb}^{-1}\text{)}$	89.1 ± 7.5	32.0 ± 2.7	19.7 ± 0.7	18.0 ± 0.7

Table I: Analysis results for the W and Z -production cross section measurement for CDF and DØ. A_V , ϵ_V and Bkg stand for acceptance, detection efficiency and Bkg, respectively, for vector boson V .

W and Z events are normally recorded using a common single lepton trigger. The event selection for W -bosons requires an isolated lepton with transverse momentum $p_T > 25 \text{ GeV}$ and $E_T > 25 \text{ GeV}$. Leptonic decays of Z -bosons are selected by imposing the same lepton quality cuts on one lepton, and looser requirements on the second lepton. Table I lists the kinematic and geometric acceptance (A_V), trigger and event selection efficiency (ϵ_V) and background (Bkg) for the electron and muon

*Work supported by the U.S. Dept. of Energy under contract DEAC02-76CHO3000

decay channel for the two experiments ($V = W$ or Z) [3, 4, 5].

The vector boson inclusive cross section times decay branching ratio follows from the number of background subtracted observed candidate events, corrected for efficiency, acceptance and luminosity:

$$\sigma \cdot B = \frac{N_{obs} - N_{bkg}}{A \epsilon \mathcal{L}}$$

Here N_{obs} is the observed number of events and N_{bkg} the number of expected background events. B indicates the branching ratio of the vector boson for the decay channel under study. The measured cross sections times branching ratio are listed in Table II and are compared with the theoretical prediction in Fig. 1. The theoretical predictions for the total production cross section, calculated to $\mathcal{O}(\alpha_s^2)$ [6], depend on three input parameters: the mass of the W -boson, taken to be $M_W = 80.23 \pm 0.18 \text{ GeV}/c^2$, the mass of the Z -boson, $M_Z = 91.188 \pm 0.002 \text{ GeV}/c^2$ [7], and the structure of the proton. Using the CTEQ2M parton distribution functions [8], the prediction for the total cross sections are $\sigma_W = 22.35 \text{ nb}$ and $\sigma_Z = 6.708 \text{ nb}$. Using the leptonic branching ratio $B(W \rightarrow \ell\nu) = (10.84 \pm 0.02)\%$, as calculated following reference [9] using the above quoted W -mass, and $B(Z \rightarrow \ell\ell) = (3.366 \pm 0.006)\%$ as measured by the LEP experiments [10], the theoretical predictions for the total inclusive production cross section times branching ratio are $\sigma_W \cdot B(W \rightarrow \ell\nu) = 2.42^{+0.13}_{-0.11} \text{ nb}$ and $\sigma_W \cdot B(Z \rightarrow \ell\ell) = 0.226^{+0.011}_{-0.009} \text{ nb}$. The two largest uncertainties on the theoretical prediction are the choice of parton distribution function (4.5%) and the uncertainty due to using a NLO parton distribution function with a full $\mathcal{O}(\alpha_s^2)$ theoretical calculation (3%). The experimental error is dominated by the uncertainty on the luminosity.

	$\sigma_W \cdot B(W \rightarrow \ell\nu)$	$\sigma_Z \cdot B(Z \rightarrow \ell\ell)$
1992-1993		
DØ (e)	$2.36 \pm 0.02 \pm 0.15$	$0.218 \pm 0.008 \pm 0.014$
DØ (μ)	$2.09 \pm 0.06 \pm 0.25$	$0.178 \pm 0.022 \pm 0.023$
CDF (e)	$2.49 \pm 0.02 \pm 0.12$	$0.231 \pm 0.006 \pm 0.011$
CDF (μ)	$2.48 \pm 0.03 \pm 0.16$	$0.203 \pm 0.010 \pm 0.012$
1994-1995		
DØ (e)	$2.38 \pm 0.01 \pm 0.22$	$0.235 \pm 0.003 \pm 0.021$
DØ (μ)	$2.28 \pm 0.04 \pm 0.25$	$0.202 \pm 0.016 \pm 0.026$

Table II: Measured cross section times branching ratio in nb for W and Z production based on integrated luminosities of 12.8 (11.4) pb^{-1} and 19.7 (18.0) pb^{-1} for the electron (muon) channel for DØ and CDF, respectively for the 1992-1993 data and the preliminary DØ results for 75.9 (32.0) pb^{-1} of data from the 1994-1995 run.

The ratio of the cross section measurements in which the error on the luminosity, common to both the W and Z events, completely cancels measures the leptonic branching ratio of the W -boson. It can be used, within the above framework, to extract the total width of the W -boson:

$$R = \frac{\sigma_W \cdot B(W \rightarrow \ell\nu)}{\sigma_Z \cdot B(Z \rightarrow \ell\ell)} = \frac{\sigma_W}{\sigma_Z} \cdot \frac{\Gamma(W \rightarrow \ell\nu)}{\Gamma(Z \rightarrow \ell\ell)} \frac{\Gamma(Z)}{\Gamma(W)}$$

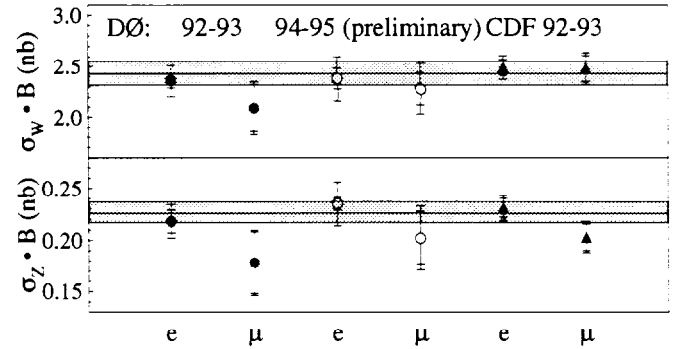


Figure 1: Measurements of the W and Z inclusive cross section compared with the theoretical prediction using the CTEQ2M parton distribution function. The shaded bands indicate the uncertainty on the predictions.

which gives

$$B^{-1}(W \rightarrow \ell\nu) = \frac{\sigma_W}{\sigma_Z} \cdot \frac{1}{B(Z \rightarrow \ell\ell)} \cdot \frac{1}{R}$$

Using the SM prediction [9] for the partial decay width $\Gamma(W \rightarrow \ell\nu)$ the total width Γ_W is given by

$$\Gamma_W = \frac{\sigma_W}{\sigma_Z} \cdot \frac{\Gamma(W \rightarrow \ell\nu)}{B(Z \rightarrow \ell\ell)} \cdot \frac{1}{R}$$

The ratio of the cross sections, using again the calculation of [6], is determined to be 3.33 ± 0.03 . The error is again dominated by the choice of parton distribution functions. Note that in the ratio the theoretical uncertainties also largely cancel. Using, as before, the measured branching ratio $B(Z \rightarrow \ell\ell) = (3.366 \pm 0.006)\%$ and the theoretical prediction for the partial decay width $\Gamma(W \rightarrow \ell\nu) = 225.2 \pm 1.5 \text{ MeV}$ [9] the W leptonic branching ratio, as determined from the combined DØ electron and muon 1992-1993 data, is $(11.02 \pm 0.5)\%$; the CDF measured branching ratio, based on the 1992-1993 electron data is $(10.94 \pm 0.33 \pm 0.31)\%$. Using the calculated partial leptonic branching ratio, these measurements yield for the width $\Gamma_W = 2.044 \pm 0.093 \text{ GeV}$ [5] and $\Gamma_W = 2.043 \pm 0.082 \text{ GeV}$ [3], respectively. The CDF value differs from their published value due to the use of more recent experimental measurements in evaluating the input parameters. Figure 2 shows the world W -width measurements together with the theoretical prediction [3, 5, 11, 12].

Taking into account that the ratio of the total cross sections σ_W/σ_Z is slightly different at a center of mass energy of 630 GeV ($\sigma_W/\sigma_Z(\sqrt{s} = 630 \text{ GeV}) = 3.26 \pm 0.09$), and accounting for the correlation between the measurements at different center of mass energies through the choice of parton distribution functions, the different values of Γ_W can be combined to give a world average of $\Gamma_W = 2.062 \pm 0.059 \text{ GeV}$, a measurement at the 3% level. This is in good agreement with the SM prediction of $\Gamma(W) = 2.077 \pm 0.014 \text{ GeV}$. The comparison of the measurement with the theoretical prediction can be used to set an upper limit on an “excess width” $\Delta\Gamma_W \equiv$

$\Gamma_W(\text{meas}) - \Gamma_W(\text{SM})$, allowed by experiment for non-SM decay processes, such as decays into supersymmetric particles or into heavy quarks. Comparing the above world average value of Γ_W with the SM prediction a 95% C.L. upper limit of $\Delta\Gamma < 109$ MeV on unexpected decays can be set.

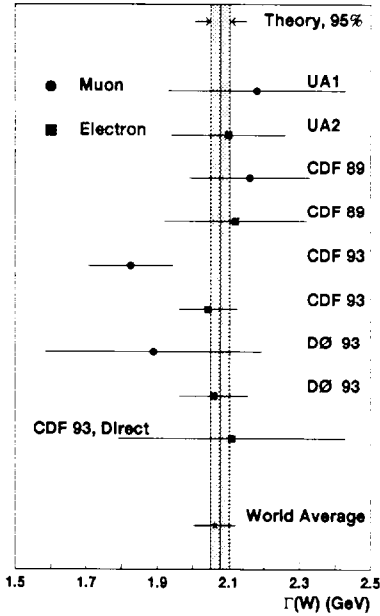


Figure 2: Measurements of Γ_W compared with the SM expectation.

Since the intermediate vector bosons are produced through a Breit-Wigner resonance the line shape of the mass distribution contains information about the width of the boson. For W -bosons, the high tail of the transverse mass distribution, where the Breit-Wigner shape dominates over the detector resolutions, can be used to extract Γ_W . Using a binned log-likelihood method, CDF has fit the transverse mass¹ (m_T) distribution far above the W pole ($m_T > 110$ GeV/ c^2) to Monte Carlo generated templates with varying W -width [13]. Using this method the W -width has been determined to be $\Gamma_W = 2.11 \pm 0.28 \pm 0.16$ GeV, where the systematic error (8%) is dominated by uncertainties in modelling the W transverse momentum distribution (6%) and the E_T resolution (5%). Although the precision of this method is currently not competitive with the extraction of the width from the ratio of cross sections, it has the advantage that it is relatively independent of SM assumptions.

III. DRELL-YAN PRODUCTION

One of the unique features of $\bar{p}p$ collisions is the large range of available partonic center of mass energies. This allows for a study of the Z line shape through the Drell-Yan process ($q\bar{q} \rightarrow (\gamma, Z) \rightarrow \ell^+\ell^-$) over a large di-lepton invariant mass region.

¹Transverse mass is defined as the invariant mass of the lepton and the neutrino of the W -decay in the transverse plane (see section V).

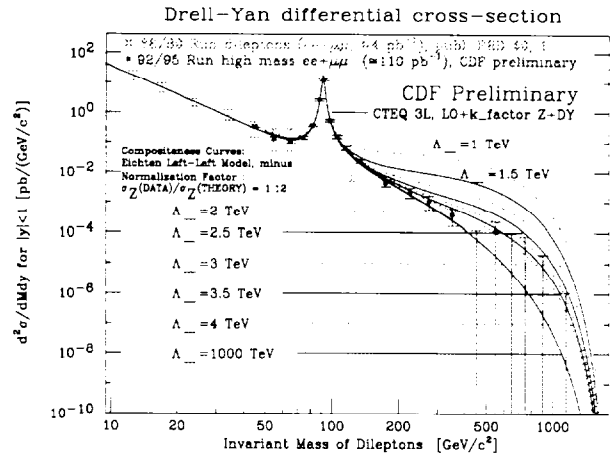


Figure 3: Double differential cross section $d^2\sigma/dM dy$ for CDF electron and muon data combined. The open symbols are from the 88/89 data. The solid symbols correspond to the full Run I data. The curves are the theoretical predictions for different Λ_- values.

The low invariant mass region allows access to the small x region of the parton distribution functions down to $x = 0.006$, where x is the fraction of the proton momentum carried by the parton. The region well above the Z pole is the region where the γZ interference effects are strongest. A possible substructure of the partons would manifest itself most prominently in a modification of the interference pattern. Substructure of partons is most commonly parametrized in terms of a contact interaction [14], characterized by a phase, η , leading to constructive ($\eta = -1$) or destructive interference ($\eta = +1$) with the SM Lagrangian, and a compositeness scale, Λ_η , indicative of the energy scale at which substructure would be revealed. By fitting the di-lepton invariant mass spectrum to various assumptions for the compositeness scale and the phase of the interference, lower limits on the compositeness scale can be set.

The CDF experiment has measured the double differential Drell-Yan cross section $d^2\sigma/dM dy$ for electron and muon pairs in the mass range $11 < M_{\ell\ell} < 150$ GeV/ c^2 for the Run 1a data [15], and $40 < M_{\ell\ell} < 550$ GeV/ c^2 for the Run 1b data. The di-electron invariant mass spectrum is measured over the rapidity interval $|\eta| < 1$. Due to a more restricted coverage, the muon cross section has been determined only over the range $|\eta| < 0.6$. Figure 3 shows the measured cross section for electrons and muons combined. The curves correspond to a leading-order calculation of the Drell-Yan cross section with in addition a contact interaction of left-handed quarks and leptons with positive interference for different values of the compositeness scale. Higher order effects have been included through the use of a constant k -factor of $k = 1.12$. The curve for $\Lambda_- = 1000$ TeV indicates the SM prediction. The data is clearly inconsistent with low Λ_- values. Performing a maximum likelihood fit yields scale factors for the electron data of $\Lambda_- \geq 3.4$ TeV, $\Lambda_+ \geq 2.4$ TeV and for the muon data of $\Lambda_- \geq 3.5$ TeV, $\Lambda_+ \geq 2.9$ TeV. Combining both channels yields $\Lambda_+ \geq 2.9$ TeV and $\Lambda_- \geq 3.8$ TeV. This implies that up to a distance of $< 10^{-17}$ cm the inter-

acting particles reveal no substructure.

IV. FORWARD-BACKWARD ASYMMETRY

Because the left-handed and right-handed coupling of fermions to the Z boson are not the same, the angular distribution of the outgoing fermion with respect to the incoming fermion in the parton center of mass frame, has a term linear in $\cos \vartheta^*$ [16]. The angular distribution is thus asymmetric and will exhibit a forward-backward asymmetry, defined as

$$A_{FB} = \frac{\sigma_F - \sigma_B}{\sigma_F + \sigma_B}$$

where σ_F is the cross section for fermion production in the forward hemisphere ($0^\circ < \vartheta^* < 90^\circ$) and, correspondingly, σ_B for the backward hemisphere ($90^\circ < \vartheta^* < 180^\circ$). Due to the changing polarization of the Z boson as function of center of mass energy, A_{FB} has a strong energy dependence. Since the couplings of the fermions to the Z boson depend on the fermion weak isospin and charge, A_{FB} is different for different initial and final states. For the Drell-Yan process $\bar{p}p \rightarrow \ell^+\ell^-$ no distinction can be made between $u\bar{u}$ and $d\bar{d}$ initial states and therefore the asymmetry measured will be a convolution of both. It is interesting to note that this process is the time-reversal of the corresponding process at e^+e^- -machines and the measurements are complementary. At LEP and SLC the measurements are free from parton distribution function uncertainties, whereas at the Tevatron, the light quark asymmetries are free from fragmentation uncertainties.

The CDF experiment has measured A_{FB} using the full Run I data set for di-electron final states with $|\eta_{\ell_1}| < 1.1$ and $|\eta_{\ell_2}| < 2.4$ [17]. The data sample is divided into two invariant mass regions: a pole region, $75 < M_{ee} < 105 \text{ GeV}/c^2$ with 5463 events and a high mass sample, $M_{ee} > 105 \text{ GeV}/c^2$ with 183 events. Figure 4 shows the event count in $\cos \vartheta^*$ for the high mass sample. The dashed line is the raw data distribution and already shows a clear forward-backward asymmetry. The points are the corrected data compared to the SM prediction using the MRSA parton distribution function [18]. The background in the pole-region is dominated by QCD di-jet events where both jets either contain or fake an electron. It has been estimated to be 110 ± 36 events. In the high mass region the background is relatively small but has a large uncertainty, 0_{-0}^{+21} events, which dominates the systematic uncertainty on the measurement in this mass region. Because of the finite mass resolution, events will migrate between the two mass regions. The deconvolution of the mass resolution is performed with a Monte Carlo simulation and results in a correction on A_{FB} of $\Delta_{A_{FB}} = +0.07 \pm 0.03$ in the high mass region and $\Delta_{A_{FB}} = -0.010 \pm 0.003$ in the pole region. The corrections for angular acceptance have also been determined from Monte Carlo simulations. The analysis yields $A_{FB} = 0.07 \pm 0.016$ for $75 < M_{ee} < 105 \text{ GeV}/c^2$, and $A_{FB} = 0.43 \pm 0.10$ for $M_{ee} > 105 \text{ GeV}/c^2$, compared to the SM predictions of $A_{FB} = 0.054 \pm 0.001$ and $A_{FB} = 0.528 \pm 0.006$, respectively.

Even though in the high mass region the asymmetry is measured with a rather large error, these measurements still serve as

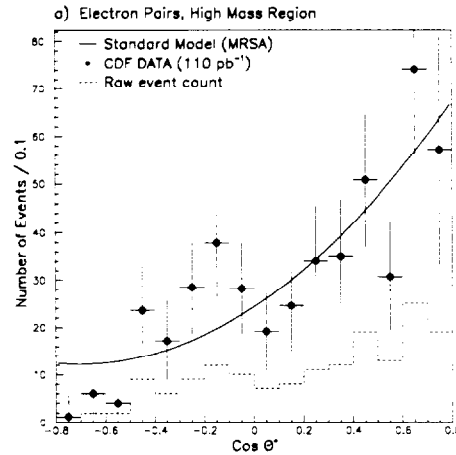


Figure 4: Distributions in $\cos \vartheta^*$ for events from the process $\bar{p}p \rightarrow Z/\gamma + X$, $Z/\gamma \rightarrow e^+e^-$ for the di-electron invariant mass region $M_{ee} > 105 \text{ GeV}/c^2$. The points are the fully corrected data and the line is the SM calculation, normalized to the number of events observed in the data. The dashed histogram is the raw event count.

a probe of extensions of the SM because models with additional heavy neutral gauge bosons can substantially alter A_{FB} . For example, Fig. 5 from [19] shows A_{FB} for $d\bar{d} \rightarrow e^+e^-$ as function of the partonic center of mass energy for the SM (solid line) and for various models with an additional neutral heavy gauge boson with a mass of $500 \text{ GeV}/c^2$. A modest event sample at a center of mass energy of $\sqrt{s} = M_{Z'}$ allowing an unambiguous sign determination of A_{FB} , would already put constraints on extended gauge sectors in the SM.

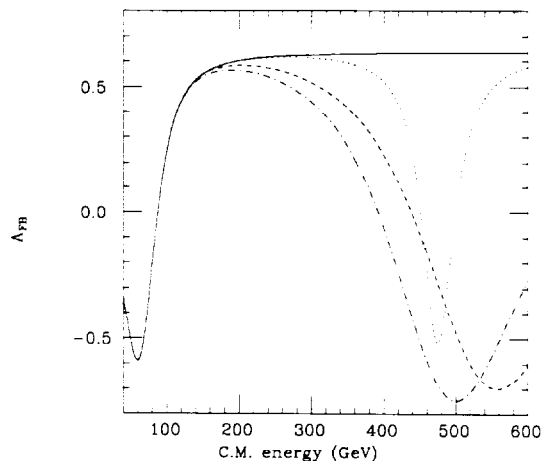


Figure 5: Parton level forward-backward asymmetry as function of center of mass energy for $d\bar{d} \rightarrow e^+e^-$ for the SM (solid line), and for models with an additional Z_I (dashed-dotted line), Z_χ (dashed line) or Z_ψ (dotted line) boson of $500 \text{ GeV}/c^2$ [19].

V. W -MASS

The mass of the W -boson is one of the fundamental parameters of the SM. A precision measurement of the W -boson mass allows for a stringent test of the radiative corrections in the SM. Combined with the measurement of the mass of the top-quark and precision measurements from e^+e^- and neutrino scattering experiments, inconsistencies between the different measurements can be looked for, possibly indicating processes beyond the SM.

In W events produced in a hadron collider in essence only two quantities are measured: the lepton momentum and the transverse momentum of the recoil system. The latter consists of the ‘‘hard’’ W -recoil and the underlying event contribution. For W -events these two are inseparable. The transverse momentum of the neutrino is then inferred from these two observables. Since the longitudinal momentum of the neutrino cannot be determined unambiguously, the W -boson mass is determined from the line shape in transverse mass, defined as

$$m_T = \sqrt{2 p_T^\ell p_T^\nu (1 - \cos \varphi^{\ell\nu})}.$$

Here $\varphi^{\ell\nu}$ is the angle between the lepton and neutrino in the transverse plane.

Both the transverse mass and lepton transverse momentum are, by construction, invariant under longitudinal Lorentz boosts. The quantity transverse mass is preferred over the lepton transverse momentum spectrum because to first order it is independent of the transverse momentum of the W . Under transverse Lorentz boosts along a direction φ^* , m_T and p_T^ℓ transform as

$$\begin{aligned} M_T^2 &\cong M_T^{*2} - \beta^2 \cos^2 \varphi^* M_L^{*2} \\ p_T^\ell &\cong p_T^{\ell*} + \frac{1}{2} \beta \cos \varphi^* M_W \end{aligned}$$

with $M_T^* = M_W \sin \vartheta^*$, $M_L^* = M_W \cos \vartheta^*$ and $\beta = \frac{p_T^W}{M_W}$. The asterisks indicate quantities in the W rest frame. The lepton transverse momentum depends linearly on β whereas the dependence of the transverse mass is second order in β . The disadvantage of using the transverse mass is that it uses the neutrino transverse momentum which is a derived quantity. The neutrino transverse momentum is equated to the missing transverse energy in the event, which is given by

$$\vec{E}_T = -\sum_i \vec{p}_{T,i} = -\vec{p}_T^e - \vec{p}_T^{e^c} - \vec{u}_T(\mathcal{L})$$

where $\vec{p}_T^{e^c}$ is the transverse momentum of the W -recoil and $\vec{u}_T(\mathcal{L})$ the transverse energy flow of the underlying event, which depends on the luminosity. It then follows that the magnitude of the missing E_T vector and the true neutrino momentum are related as $E_T = p_T^\nu + \frac{1}{4} \frac{u_T^2}{p_T^2}$. This relation can be interpreted as the definition of the neutrino momentum scale. Note that the underlying event gives rise to a bias in the measured neutrino momentum with respect to the true neutrino momentum. When there are more interactions per crossing $|\vec{u}_T|$ behaves as a two-dimensional random walk and is proportional to $\sqrt{I_C}$, where I_C

is the number of interactions per crossing. The shift in measured neutrino momentum is thus directly proportional to the number of interactions per crossing. The resolution increases as $\sqrt{I_C}$. At high luminosities alternate methods to determine the W -mass may therefore be advantageous [20].

Since there is no analytic description of the transverse mass distribution, the W -mass is determined by fitting Monte Carlo generated templates in transverse mass for different masses of the W -boson to the data distribution. This distribution exhibits a Jacobian edge characteristic of two-body decays which contains most of the mass information. For the W -mass determination both the energy scale for the lepton and recoil system, which determine the peak position of the transverse mass distribution, as well as the resolutions on the measured variables, which control the steepness of the Jacobian edge, are crucial.

The CDF mass analysis discussed here is based on the Run 1a data [21]. The $D\bar{O}$ mass analysis also includes a preliminary result from the Run 1b data [22]. In the CDF W -mass analysis the momentum scale of the central magnetic tracker is set by scaling the measured J/ψ -mass to the world average value using $J/\psi \rightarrow \mu^+ \mu^-$ decays. Based on a sample of approximately 60,000 events a scale factor of 0.99984 ± 0.00052 has been derived. The dominant contribution to the error comes from the uncertainty in the amount of material the muons traverse. This procedure establishes the momentum scale at the J/ψ -mass, where the average muon p_T is about 3 GeV/c, and needs to be extrapolated to the momentum range appropriate for leptons from W -decays. The error due to possible nonlinearities in the momentum scale is addressed by studying the measured J/ψ -mass as function of $\langle 1/p_T^2 \rangle$, extrapolated to zero curvature. This extrapolation, which includes an uncertainty on a possible non-linearity of the momentum measurement, increases the error on the momentum scale to 0.00058 at the W -mass. This results in an error on the W -mass of 50 MeV/c².

Having established the momentum scale, the calorimeter energy scale is determined from a line shape comparison of the observed E/p distribution with a detailed Monte Carlo prediction as shown in Fig. 6. A two-dimensional fit of Monte Carlo generated E/p distributions in the energy scale and the electron momentum resolution is used to establish the absolute calorimeter energy scale. The scale factor is extracted from a fit over the range $0.9 < E/p < 1.1$. Since the momentum measurement is very sensitive to bremsstrahlung effects, the energy scale determination is critically dependent on an accurate modelling of the amount of material the electrons traverse. Using the ratio of events in the region $1.3 < E/p < 2.0$ to the events in the range $0.8 < E/p < 1.2$ the amount of material is determined to be $(8.9 \pm 0.9)\% X_0$, consistent with independent checks using photon conversions and Z -events but slightly higher than from a direct accounting of the material. The limited statistics in the high E/p region is the dominant source of the systematic error on the amount of material traversed by electrons and thus on the energy scale determination. The uncertainty of 10% on the amount of material in front of the calorimeter contributes a 70 MeV/c² uncertainty on the W -mass. The other two main contributions to the total energy scale error are a 65 MeV/c² error due to the statistics in the E/p -peak and a 50 MeV/c² error from the uncer-

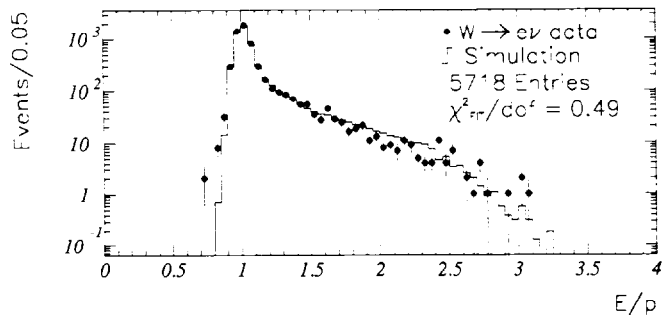


Figure 6: The E/p distribution for electrons in the W -sample (points) with the best fit from the simulation (histogram).

tainty on the electron resolution. The total error on the W -mass from setting the energy scale using the momentum scale is thus $110 \text{ MeV}/c^2$ which, combined with the $50 \text{ MeV}/c^2$ momentum scale uncertainty, gives a total energy scale uncertainty on the W -mass of $120 \text{ MeV}/c^2$ for the measurement using $W \rightarrow e\nu$ decays.

The energy and momentum scales are verified by measuring the masses of known resonances, the Z -mass and the masses of the Υ resonances. They are all in good agreement with the world average values. The width of the Z -resonance provides a constraint on the momentum resolution that results in a systematic error on the W -mass from the uncertainty on the momentum and energy resolution of $60 \text{ MeV}/c^2$ and $80 \text{ MeV}/c^2$ for the muon and electron measurement, respectively. The hadronic energy scale does not need to be determined separately since $Z \rightarrow e^+e^-$ collider events are used to model the W -recoil system.

At $D\bar{O}$ the W -mass is measured from $W \rightarrow e\nu$ decays. The electromagnetic (EM) energy scale is determined by calibrating to the $Z \rightarrow ee$ resonance. Since the absolute energy scale of the EM calorimeter is not known with the required precision, the ratio of the measured W and Z masses and the world average Z mass are used to determine the W boson mass. The W mass measured is de facto the ratio of the measured W and Z mass, scaled to the LEP Z mass: $M_W = \frac{M_W^{D\bar{O}}}{M_Z^{LEP}} \times M_Z^{LEP}$. A number of systematic effects, common to both measurements, cancel in the ratio. Most notably, as shall be discussed in more detail below, the ratio is to first order insensitive to the absolute energy scale.

Test beam measurements have demonstrated the EM calorimeter to be linear to better than 0.5% for electron energies exceeding 10 GeV. To establish the energy scale with the precision required for this measurement, it is necessary to determine to which extent a potential offset in the energy response, as opposed to a scale factor, is responsible for the deviation of the ratio $\frac{M_W^{D\bar{O}}}{M_Z^{LEP}}$ from unity. This was achieved by combining the measured Z mass with the measurements of $\pi^0 \rightarrow \gamma\gamma$ and $J/\psi \rightarrow e^+e^-$ decays and comparing them to their known values [23]. If the electron energy measured in the calorimeter

and its true energy are related by $E_{\text{meas}} = \alpha E_{\text{true}} + \delta$, the measured and true mass values are, to first order, related by $m_{\text{meas}} = \alpha m_{\text{true}} + \delta f$. The variable f depends on the decay topology and is given by $f = \frac{2(E_1 + E_2)}{m_{\text{true}}} \sin^2 \gamma/2$, where γ is the opening angle between the two decay products and E_1 and E_2 are their measured energies.

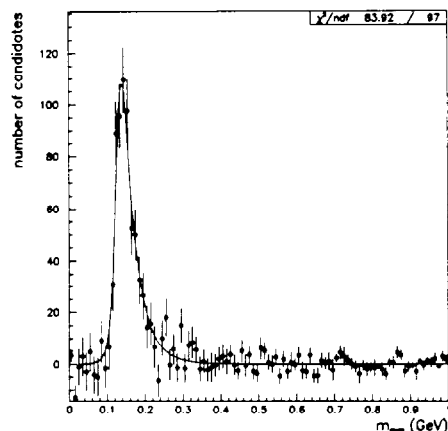


Figure 7: The M_{sym} mass spectrum obtained from $\pi^0 \rightarrow \gamma\gamma$ decays.

Figure 7 shows the background subtracted mass spectrum of the decay $\pi^0 \rightarrow \gamma\gamma$. The two photons in the decay of the neutral pion are not resolved in the calorimeter, but by selecting events in which both γ 's convert into an e^+e^- -pair, and produce distinctive doubly ionizing tracks in the central detector, the opening angle can be reconstructed. The “mass” plotted in Fig. 7 (data points with error bars) is

$$M_{\text{sym}} = E \cdot \sin \frac{\vartheta}{2}, \quad (1)$$

where E is the cluster energy, equal to the sum of the photon energies, and ϑ is the opening angle of the two photons. M_{sym} is equal to the invariant mass for symmetric decays. The shape compares well with the Monte Carlo simulation shown as the solid line. The measured mass is $M_{\pi^0} = (135.4 \pm 10.0) \text{ MeV}/c^2$. The sensitivity to the energy scale and offset is determined by varying both parameters in a Monte Carlo simulation and performing a χ^2 fit to the data. This procedure maps out an allowed region in the (α, δ) -plane shown as the dashed line in Fig. 8.

Similarly, a J/ψ signal with a significance of about 5σ has been extracted from the data, which yields an additional, independent constraint on α and δ (dashed-dotted line in Fig. 8). The strongest constraint on the energy scale uncertainty comes from the Z data. The fact that electrons from Z decays are not monochromatic is exploited by studying the invariant mass distribution as function of the variable f . Small values of f correspond to the decay of highly boosted Z bosons with, on average, higher energies. The dependence of the observed Z boson mass as function of f thus directly translates into a constraint on the energy scale and offset, shown as the solid line in Fig. 8. Each of

the mass states has a different sensitivity to α and δ and, taken together, provide a powerful tool for establishing the energy scale in situ. When combined, these three constraints limit α and δ to the shaded elliptical region. Test beam measurements permit a small nonlinear term in the energy response, which affects both α and δ and alters the ratio M_W/M_Z largely through the effect on δ . The allowed region in the (α, δ) -plane when nonlinearities are included is indicated by the dotted line in Fig. 8.

Using the measured masses for the observed resonances, the energy scale factor determined for the Run Ia data is $\alpha = 0.9514 \pm 0.0018_{-0.0017}^{+0.0061}$ and the offset is $\delta = (-0.158 \pm 0.015_{-0.21}^{+0.03})$ GeV, where the asymmetric errors are due to possible calorimeter nonlinearities. The measured offset is consistent with that determined from test beam data, and has been confirmed by a detailed Monte Carlo study of energy loss in the central detectors. The dependence of the measured ratio of the W mass to Z mass on α and δ may be estimated from

$$\left. \frac{M_W(\alpha, \delta)}{M_Z(\alpha, \delta)} \right|_{\text{meas}} = \left. \frac{M_W}{M_Z} \right|_{\text{true}} \left[1 + \frac{\delta}{\alpha} \cdot \frac{f_W M_Z - f_Z M_W}{M_Z \cdot M_W} \right].$$

It should be noted that the W mass is insensitive to α if $\delta = 0$. The offset results in a 5 MeV/c² correction to the measured W mass. The uncertainty on the absolute energy scale results, for the Run Ia data sample, in an uncertainty on M_W of 160 MeV/c², of which 150 MeV/c² is due to the limited Z statistics. For the Run Ib data sample, with a total integrated luminosity of approximately 76 pb⁻¹, the energy scale uncertainty on the W mass is 80 MeV/c².

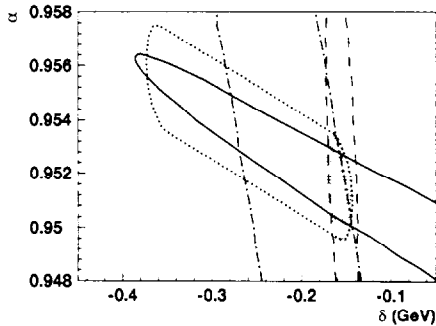


Figure 8: Constraints on slope α and intercept δ from observed $J/\psi \rightarrow e^+e^-$ (dashed-dotted line), $\pi^0 \rightarrow \gamma\gamma$ (dashed line), and $Z \rightarrow e^+e^-$ decays (solid line). The shaded inner contour shows the combined result. The dotted line indicates the allowed area when nonlinear terms, as constrained by test beam measurements, are included.

The W event sample is selected by placing very stringent kinematic and fiducial cuts. Both the CDF and DØ mass analyses are currently based on event samples with central leptons only. The main difference in event selection is the treatment of the hadronic activity in the event. The CDF event selection excludes events with jets with $E_T > 30$ GeV. In addition p_T^W is required to be less than 20 GeV/c, whereas DØ only requires $p_T^W < 30$ GeV/c. These sets of selection criteria yield event

samples of 8049 and 4663 events for the electron and muon decays, respectively, for CDF and 7234 $W \rightarrow e\nu$ decays for the Ia and 32856 for the Ib data set for DØ.

The W -mass is then determined from a maximum likelihood fit of Monte Carlo generated templates in transverse mass to the data distributions. In the Monte Carlo model of W -production, events are generated according to a relativistic Breit-Wigner resonance, with a longitudinal momentum distribution as given by the chosen parton distribution function. The CDF choice for nominal parton distribution function is the MRSD'-pdf [18]. In their model the transverse momentum of the W is generated according to the measured p_T distribution of Z -events. This procedure can be justified because of the similarity between W and Z -production and because there are large uncertainties, both theoretical as well as experimental, on the W p_T -distribution. The procedure has an added advantage that the recoil system does not need to be modeled independently, since it is taken directly from Z -events with the two leptons removed. This recoil distribution from Z -events is corrected for the lepton removal and modified to match data and Monte Carlo with respect to the width of the distribution of the projection of the p_T of the recoil system perpendicular to the lepton direction. The disadvantage of the method is that very few events (555 events to be precise) are used to model the recoil with a slightly different acceptance than for W -events, and it ignores the correlation between the transverse and longitudinal momenta and the difference in mass between the W and Z -bosons.

The DØ experiment generates W bosons using the double differential production cross section in p_T and rapidity calculated at next to leading order [24] using the MRSA parton distribution functions [18], thus including the correlation between the longitudinal and transverse momentum. Minimum bias events are used to model the underlying event, mimicking the debris in the event due to spectator parton interactions and the pile-up associated with multiple interactions, and including the residual energy from previous beam crossings. The relative response of the hadronic and EM calorimeters is established by studying Z events. To ensure an equivalent event topology between the W and Z events, Z decays in which one electron is in the end calorimeter are included in this study. The transverse momentum balance in Z events is given by $\vec{p}_T^{e_1} + \vec{p}_T^{e_2} + \vec{p}_T^{ec} + \vec{u}_T = -\vec{E}_T$. One finds for the average $|\vec{p}_T^{e_1} + \vec{p}_T^{e_2} + \vec{E}_T|^2 = \kappa^2 |\vec{p}_T^{ee}|^2 + |\vec{u}_T|^2$ assuming $|\vec{p}_T^{ec}| = \kappa |\vec{p}_T^{ee}|$, where \vec{p}_T^{ee} is the transverse momentum of the Z measured from the two electrons. The cross term on the right hand side averages to zero since the underlying event vector is randomly distributed with respect to the Z recoil system. Figure 9a shows the distribution of $|\vec{p}_T^{e_1} + \vec{p}_T^{e_2} + \vec{E}_T|^2$ versus $|\vec{p}_T^{ee}|^2$. The data shows a linear relation between the EM and hadronic energy scale, and yields $\kappa = 0.83 \pm 0.04$. The intercept yields the magnitude of the underlying event vector, $|\vec{u}_T| = 4.3 \pm 0.3$ GeV/c, consistent with the value obtained from minimum bias events. The uncertainty on M_W due to the uncertainty on the hadronic energy scale is 50 MeV/c² for the Run Ia data.

The modeling of the recoil and underlying event are verified and constrained by comparing the p_T of the Z obtained from the two electrons, \vec{p}_T^{ee} , to that obtained from the rest of the event:

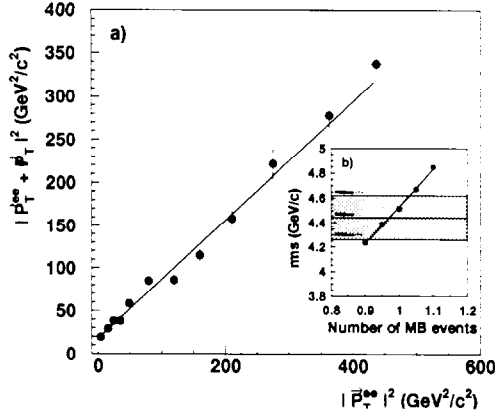


Figure 9: a) Distribution of $|\vec{p}_T^{e1} + \vec{p}_T^{e2} + \vec{E}_T|^2$ versus $|\vec{p}_T^{ee}|^2$ for Z events; b) Sensitivity of the width of the distribution in $\vec{p}_T^{ee} + \vec{p}_T^{ee} + \vec{u}_T$, projected along the bi-sector of the two electrons, on the number of minimum bias events. The band corresponds to the $\pm 1\sigma$ uncertainty on this measurement.

$-\vec{p}_T^{ee} - \vec{u}_T$. To minimize the contribution from the electron energy resolution, the vector sum of these two quantities is projected along the bisector of the two electron directions. Since \vec{u}_T is randomly oriented and has a magnitude $\sim p_T^Z$, the width of the distribution is sensitive to the underlying event contribution while the mean is largely unaffected. The sensitivity of the width of this distribution to the mean number of minimum bias events that mimic the underlying event is determined by varying the number of minimum bias events in the Monte Carlo, as shown by the points in Fig. 9b. For the Ia data, the number of minimum bias events preferred is 0.98 ± 0.06 , consistent with one. The uncertainty on M_W from the underlying event model is $60 \text{ MeV}/c^2$.

The mass of the W is obtained from a maximum likelihood fit over the transverse mass range $65 < m_T < 100 \text{ GeV}/c^2$ ($60 < m_T < 90 \text{ GeV}/c^2$) for CDF (DØ). Figures 10 and 11 show the transverse mass distributions for the data together with the best fit of the Monte Carlo for the Run Ib electron data for DØ and for the muon and electron channel for Run Ia for CDF, respectively. The W -mass is determined to be $M_W^\mu = 80.310 \pm 0.205(\text{stat}) \pm 0.130(\text{sys}) \text{ GeV}/c^2$ based on 3268 $W \rightarrow \mu\nu$ events in the mass fitting window and $M_W^e = 80.490 \pm 0.145(\text{stat}) \pm 0.175(\text{sys}) \text{ GeV}/c^2$ based on 5718 events for CDF. DØ finds $M_W^e = 80.350 \pm 0.140(\text{stat.}) \pm 0.165(\text{syst.}) \pm 0.160(\text{scale}) \text{ GeV}/c^2$ based on 5982 events in the mass fitting window using the Ia data, and $M_W^e = 80.380 \pm 0.070(\text{stat.}) \pm 0.130(\text{syst.}) \pm 0.080(\text{scale}) \text{ GeV}/c^2$ based on 27040 events for the Ib data. Table III lists the systematic errors on the individual measurements and the common errors.

The dominant theoretical uncertainty in this measurement comes from the p_T^W model and the uncertainty on the proton structure. Parton distributions and the spectrum in p_T^W are correlated. The DØ experiment has addressed this correlation in the determination of its uncertainty on the W mass. In their analysis new parametrizations of the CTEQ 3M parton distribution func-

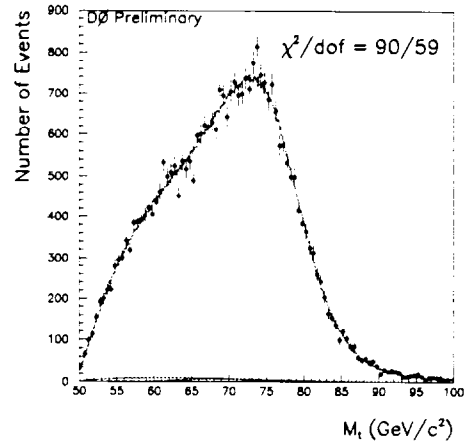


Figure 10: DØ transverse mass distribution of $W \rightarrow e\nu$ decays collected during the 1994-1995 run. The points are the data and the line is the best fit.

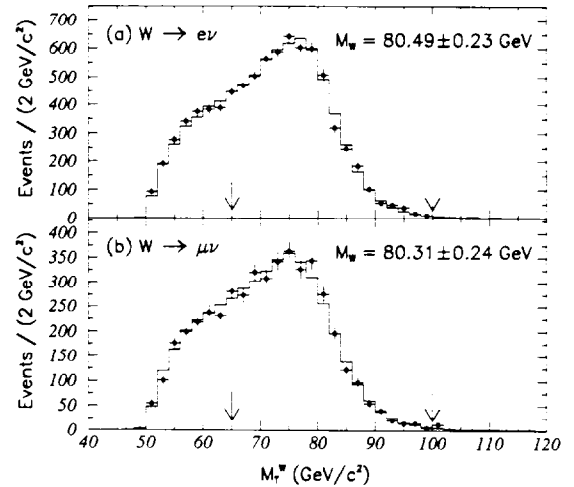


Figure 11: Transverse mass distribution of $W \rightarrow e\nu$ (top) and $W \rightarrow \mu\nu$ (bottom) decays from CDF. The points are the data and the histogram is the best fit to the data. The arrows indicate the range used to extract the W -mass.

tion were obtained that included in the fit the CDF W asymmetry data from Run Ia [25], where all data points had been moved coherently up or down by one standard deviation. In addition one of the parameters, which describes the Q^2 -dependence of the parametrization of the non-perturbative functions describing the p_T^W spectrum [24], was varied. The constraint on this parameter was provided by the measurement of the p_T^Z spectrum. The

	CDF			DØ		
	e	μ	common	Ia	Ib	common
Statistical	145	205	—	140	70	—
Energy scale	120	50	50	160	80	25
Angle scale	—	—	—	50	40	40
E or p resolution	80	60	—	70	25	10
p_T^W and recoil model	80	75	65	110	95	—
pdf's	50	50	50	65	65	65
QCD/QED corr's	30	30	30	20	20	20
W -width	20	20	20	20	10	10
Backgrounds	10	25	—	35	15	—
Efficiencies	0	25	—	30	25	—
Fitting procedure	10	10	—	5	5	—
Total	230	240	100	270	170	80
Combined	180			150		

Table III: Errors on M_W in MeV/c^2 .

uncertainty due to parton distribution functions and the p_T^W input spectrum was then assessed by varying simultaneously these new parton distribution function and the parameter describing the non-perturbative part of the p_T^W spectrum. A total error on the W -mass of $65 \text{ MeV}/c^2$ has been assigned due to these uncertainties.

The CDF experiment uses their measurement of the W charge asymmetry as the sole constraint on the uncertainty due to the p_T^W and parton distribution functions. Figure 12 shows the correlation between ΔM_W and the significance of the deviation of the theoretical prediction for the W -asymmetry and the data for the electron and muon channel separately (cf. eq. (2)). The uncertainty on M_W is taken to be the symmetrized spread in masses for $-2 < \zeta < 2$, being $50 \text{ MeV}/c^2$.

Combining [26] these measurements with previous W mass measurements [27], assuming the only correlated uncertainty between the measurements is due to the parton distribution functions, gives a world average of $M_W = 80.356 \pm 0.125 \text{ GeV}/c^2$.

An indirect measurement of the W -mass, through the measurement of the weak mixing angle $\sin^2 \vartheta_W$, is obtained from the study of νN deep inelastic scattering experiments. The CCFR experiment studies ν_μ -nucleon interactions and the ratio of charged and neutral current cross sections provides a direct measurement of the weak mixing angle. The cross sections have large contributions from electroweak radiative corrections. In the “on shell” scheme, however, where $\sin^2 \vartheta_W$ is defined as $1 - \frac{M_W^2}{M_Z^2}$ to all orders, these corrections largely cancel in the ratio, thus reducing the dependence on the top mass and Higgs mass significantly and providing an indirect measurement of M_W . A preliminary value of $\sin^2 \vartheta_W = 0.2213 \pm 0.0021(\text{stat.}) \pm 0.0027(\text{syst.}) \pm 0.0034(\text{model})$ has been reported [28], corresponding to a W mass value of $M_W = (80.46 \pm 0.25) \text{ GeV}/c^2$. The largest contribution to the systematic uncertainty comes from the uncertainty on the flux of background ν_e 's. The model uncertainty is dominated by the turn-on of the charm quark production cross section. The latter uncertainty is expected to be

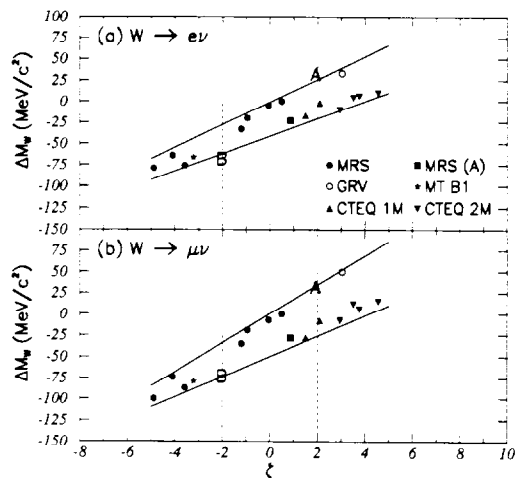


Figure 12: Correlation between ΔM_W and ζ , the significance of the difference between data and theory for the W -charge asymmetry, for various parton distribution functions for the (a) $W \rightarrow e\nu$ - and (b) $W \rightarrow \mu\nu$ -sample. The nominal mass measurement uses the MRSD'— parton distribution function.

reduced substantially with the follow-up experiment NuTeV, which will be able to measure the cross sections with neutrino and anti-neutrino beams separately.

VI. W -CHARGE ASYMMETRY

As Fig. 12 shows, the W mass is strongly correlated with the parton distribution functions. The parton distribution functions can be constrained at the appropriate Q^2 -scale by measuring the charge asymmetry in W -production itself. The two, partly

compensating, sources that contribute to the W -charge asymmetry are the production and decay processes. Since on average a u -quark carries more momentum than a d -quark, more W^+ -bosons are produced along the proton direction than along the anti-proton direction resulting in a production charge asymmetry defined as

$$A(y_W) = \frac{dN^+(y_W)/dy - dN^-(y_W)/dy}{dN^+(y_W)/dy + dN^-(y_W)/dy}$$

The W -rapidity, y_W , however, cannot be reconstructed unambiguously because of the two-fold ambiguity in the longitudinal momentum of the neutrino. The quantity that is measured experimentally is the decay lepton charge asymmetry, defined as

$$A(y_\ell) = \frac{dN^+(y_\ell)/dy_\ell - dN^-(y_\ell)/dy_\ell}{dN^+(y_\ell)/dy_\ell + dN^-(y_\ell)/dy_\ell}$$

where $N^{+(-)}$ is the number of positively (negatively) charged leptons detected at pseudorapidity y_ℓ . Since the rapidity of the decay lepton is measured, there is an additional contribution from the $V - A$ coupling of the W . Since W -bosons are produced through $q\bar{q}$ annihilation they are almost fully polarized and the lepton from, for example, the W^+ -decay is preferentially emitted along the anti-proton direction, which partially undoes the production asymmetry. Because of CP symmetry, $A(+y) = -A(-y)$, the measured asymmetries at positive and negative rapidities can be combined to get a statistically more powerful measurement. The $V - A$ structure of the W -decay is very well understood. Thus, the charge asymmetry measurement can be used to probe the structure of the proton in the x range 0.007 to 0.27.

The CDF experiment, based on an integrated luminosity of about 20 pb^{-1} measured the charge asymmetry for W -decays into electrons and muons and constrained the then current parton distribution functions [25]. The lepton pseudorapidity range in that analysis was $|\eta| < 1.0$ for muons and $|\eta| < 2.4$ for electrons. It was limited by the rapidity coverage provided by the central tracking chamber. The analysis has been updated [29] using the full Run 1 data set with a total integrated luminosity of 110 pb^{-1} . The rapidity coverage for muons has been extended by utilizing the forward muon toroids [30] covering $1.95 < |\eta| < 3.6$, which collected 72 pb^{-1} of data. The efficiency for electrons in the plug calorimeter ($1.1 < |\eta| < 2.4$) was also substantially improved. In the previous analysis only the central tracking chamber was used in the electron identification. Because of the limited coverage of this tracking system almost no tracks were reconstructed beyond $|\eta| \approx 1.8$. In the new analysis, utilizing the silicon vertex detector (SVX) and the vertex chamber, an average track finding efficiency of 60%, almost uniform in η , has been obtained out to rapidities of $|\eta| \approx 2.3$. For the high η region, though, the electron charge cannot be determined by the tracking system alone. In this region the charge is determined from a comparison of the φ -angle as determined from the SVX track, and from the calorimeter energy deposition. At the location of the calorimeter an average displacement of 0.5 cm is expected in the pseudorapidity range $1.2 < |\eta| < 1.8$, which is measured with a resolution of 0.15 cm.

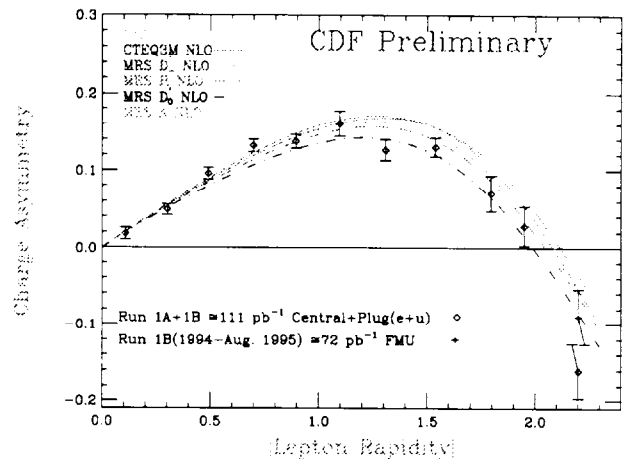


Figure 13: CDF Run I measured lepton charge asymmetry from $W \rightarrow \ell\nu$ events compared to NLO predictions for different parton distribution functions.

Figure 13 shows the measured asymmetry as a function of the lepton rapidity together with the theoretical prediction for different parton distribution functions. The predictions were obtained using the DYRAD NLO Monte Carlo [31]. Compared to the previous analysis the new measurements at high rapidity should be noted. Since the measurement is a ratio measurement, many systematic errors cancel and the total systematic error is about 20% of the statistical error.

The asymmetry measurement provides an independent discriminant between different parton distribution functions. The disagreement between theory and experiment can be quantified by defining the significance of the disagreement between the weighted mean asymmetry (\bar{A}) from theory and experiment as

$$\zeta = \frac{\bar{A}_{pdf} - \bar{A}_{data}}{\sigma(\bar{A}_{data})} \quad (2)$$

The ζ values listed in Table IV seem to prefer the recent MRS parton distribution functions [18] over other distributions [8, 32]. The constraint which the W charge asymmetry provides on the uncertainty on the W mass measurement, however, is not expected to scale with event statistics, since the measurement is mainly sensitive to the slope of the ratio of the u and d parton distribution functions and does not probe the full parameter range describing them.

PDF Set	ζ
CTEQ3M	1.16
MRS A, G	1.75
MRS H	-0.51
MRSD'	0.68
GRV 94	2.59
GRV 92	4.13

Table IV: Comparison between measured and predicted asymmetry for different parton distribution functions.

VII. RARE W DECAYS

The study of rare decays provides a precision test of the underlying theory since in general the predictions of rare decay rates involve higher order calculations. W decays into a pseudoscalar meson and a photon, $W \rightarrow P\gamma$, are particularly attractive since they are sensitive to new physics which affects the $WW\gamma$ vertex. A search for $W \rightarrow P\gamma$ decays thus complements di-boson analyses described in detail in the following section.

Currently, experiments have only looked for the rare decay $W \rightarrow \pi\gamma$ [33, 34, 35] with the strongest limit coming from the latest CDF analysis. In this analysis, based on an integrated luminosity of 16.7 pb^{-1} , events were selected with an energetic photon and a single central jet with $E_T > 15 \text{ GeV}$ with a matching isolated track. The track was required to have $p_T > 15 \text{ GeV}/c$ with no other charged tracks with $p_T > 1 \text{ GeV}/c$ in a cone of radius $\Delta R = 0.7$. By initially not placing a cut on the electromagnetic fraction of the pion jet, the sample is dominated by isolated electrons and permits measurement of many of the efficiencies from the data itself. In the final selection the electromagnetic fraction of the jet is required to be less than 80% of the total jet energy, and a sample of 79 events remains (see Fig. 14) with one event in the search region $|M(\pi\gamma) - M_W| < 8.1 \text{ GeV}/c^2$.

The background, primarily coming from jet production with the jet opposite the photon candidate fragmenting into a single charged particle, possibly associated with neutrals, has been estimated to be $2.6 \pm 1.0 \pm 1.3$ events in the mass window. The one event observed is thus consistent with background. Without background subtraction, the 95% confidence level limit is 4.9 events. Using the measured W production cross section, this results in a 95% CL upper limit on the partial decay width of

$$\frac{\Gamma(W \rightarrow \pi^\pm\gamma)}{\Gamma(W \rightarrow e\nu)} < 2 \cdot 10^{-3},$$

to be compared with the theoretical prediction of [36] $\Gamma(W \rightarrow \pi^\pm\gamma)/\Gamma(W \rightarrow e\nu) \sim 3 \cdot 10^{-8}$.

VIII. GAUGE BOSON PAIR PRODUCTION

Similar to a study of rare decays of vector bosons, a study of the magnetic dipole and electric quadrupole moments of the W boson probes the W interaction vertex. The non-Abelian $SU(2) \times U(1)$ gauge symmetry of the SM implies that the gauge bosons self-interact. These self-interactions give rise to very subtle interference effects in the SM and the couplings are uniquely determined by the gauge symmetry in order to preserve unitarity. The magnetic dipole and electric quadrupole moments of the W are, in the SM at tree level, given by:

$$\mu_W = \frac{e}{m_W} \quad Q_W^* = \frac{-e}{m_W^2}.$$

The most general effective electroweak Lagrangian, invariant under $U(1)_{EM}$, however, contains eight independent coupling parameters, the CP -conserving parameters κ_V and λ_V and the CP -violating parameters $\tilde{\kappa}_V$ and $\tilde{\lambda}_V$, where $V = \gamma$ or Z . The CP -conserving parameters are related to the magnetic dipole

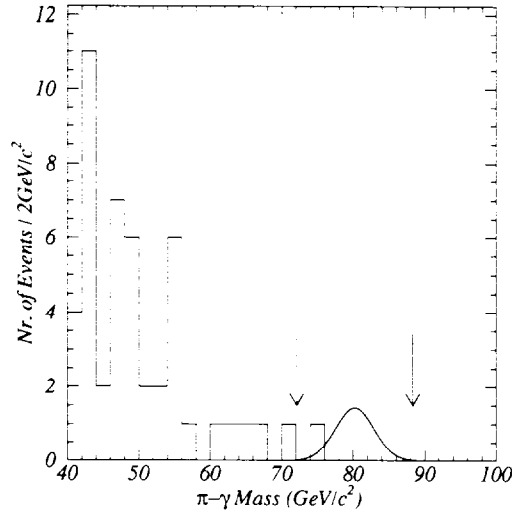


Figure 14: The CDF distribution in $M(\pi\gamma)$ for the search for the rare decay $W \rightarrow \pi\gamma$. The arrows indicate the search window. The Gaussian, centered at M_W , corresponds to the 95% CL limit of 4.9 events.

(μ_W) and electric quadrupole (Q_W^e) moments of the W boson, while the CP -violating parameters are related to the electric dipole (d_W) and the magnetic quadrupole (Q_W^m) moments [37]:

$$\begin{aligned} \mu_W &= (e/2m_W)(1 + \kappa_\gamma + \lambda_\gamma), \\ Q_W^e &= (-e/m_W^2)(\kappa_\gamma - \lambda_\gamma), \\ d_W &= (e/2m_W)(\tilde{\kappa}_\gamma + \tilde{\lambda}_\gamma), \\ Q_W^m &= (-e/m_W^2)(\tilde{\kappa}_\gamma - \tilde{\lambda}_\gamma). \end{aligned}$$

In the SM the couplings at tree level are given by $\kappa_V = 1$ ($\Delta\kappa_V = \kappa_V - 1 = 0$), $\lambda_V = \tilde{\kappa}_V = \tilde{\lambda}_V = 0$. Because of the similarity of the CP -conserving and CP -violating terms in the Lagrangian, the kinematic behavior of these terms is similar and the limits on both sets of anomalous couplings will be approximately the same. Therefore CP -violating terms will not be discussed explicitly. Also, unless stated, it will be assumed that $\Delta\kappa_\gamma = \Delta\kappa_Z$ and $\lambda_\gamma = \lambda_Z$.

A direct measurement of the moments of the W boson, and thus of the gauge boson self-interactions, is possible through the study of gauge boson pair production. The cross sections for di-boson production, however, are all extremely small. For example, the predicted cross section times branching ratio for W -pair production with $WW \rightarrow \ell\nu\nu$ ($\ell = e, \mu$) is about 0.5 pb and large integrated luminosities would be needed for a significant measurement of the gauge couplings. The SM process of W -pair production, however, is characterized by large cancellations between the s and t channel production processes. The contributions from the t channel diagrams by themselves would violate unitarity. This implies that if the couplings deviate even modestly from their SM values, the gauge cancellations are destroyed and a large increase of the cross section is observed. Moreover, the differential distributions will be modified giving rise to gauge bosons with a large transverse boost since

the largest gauge cancellations occur for highly boosted bosons.

A WWV interaction Lagrangian with constant anomalous couplings would thus violate unitarity at high energies and therefore the coupling parameters must be modified to include form factors [38], that is, $\Delta\kappa(\hat{s}) = \Delta\kappa/(1 + \hat{s}/\Lambda^2)^2$ and $\lambda(\hat{s}) = \lambda/(1 + \hat{s}/\Lambda^2)^2$, where \hat{s} is the square of the center of mass energy of the subprocess. Λ is a unitarity preserving form factor scale and indicates the scale at which the SM predictions are probed. In the next subsections different types of gauge boson pair production will be discussed.

A. W Pair Production

DØ has searched for W -boson pair production $\bar{p}p \rightarrow WW + X \rightarrow \ell\ell'\nu\nu'$ ($\ell\ell' = ee/e\mu/\mu\mu$) [39]. The standard selection criteria for W -events have an overall efficiency for W -pair production of ≈ 0.07 and with an integrated luminosity of $\mathcal{L} \approx 14 \text{ pb}^{-1}$ 0.47 ± 0.07 events are expected from SM processes. The most significant background to this process is $t\bar{t}$ production. Because of the additional two b -jets in $t\bar{t}$ events, this background can be eliminated in a straightforward way by a cut on the hadronic activity in the event. DØ applies a cut on the p_T of the WW -system, $E_T^{HAD} = |-(\vec{E}_T^{\ell_1} + \vec{E}_T^{\ell_2} + \vec{E}_T)|$, which is required to be less than 40 GeV. This requirement rejects about 75% of the $t\bar{t}$ background and has an efficiency of 95% for the expected WW signal. The searches in the $ee\nu\nu$, $e\mu\nu\nu$ and $\mu\mu\nu\nu$ channels yield one signal event with an anticipated background of 0.56 ± 0.13 events. An upper limit on the W -pair production cross section of $\sigma(WW) < 87 \text{ pb}^{-1}$ has been set at 95% CL.

With larger integrated luminosities it is possible to measure the W -pair production cross section. Based on an integrated luminosity of $\mathcal{L} = 108 \text{ pb}^{-1}$ CDF has done an analysis similar to the DØ analysis searching for W -pairs in the di-lepton channel using a jet veto, that is, events with jets with $E_T > 10$ GeV are rejected. The selection yields 5 signal events on a background of 1.2 ± 0.3 events. The measured W -pair production cross section is $\sigma(\bar{p}p \rightarrow WW) = (10.2_{-5.1}^{+6.3} \pm 1.6) \text{ pb}$, where the SM predicts $\sigma_{SM}(\bar{p}p \rightarrow WW) = (9.5 \pm 1.0) \text{ pb}$. It should be pointed out that the smallness of the cross sections in itself is a beautiful demonstration of the gauge cancellations in the SM.

Since the cross section increases very rapidly when the couplings deviate from their SM values, the measured 95% CL upper limit on the cross section can be used to set limits on anomalous couplings. Figure 15 shows the CDF 95% CL exclusion contours in $\Delta\kappa$ and λ for two different form factor scales, assuming $\lambda_\gamma = \lambda_Z$ and $\Delta\kappa_\gamma = \Delta\kappa_Z$. It is customary to quote limits on only one coupling, keeping the other couplings fixed to their SM value. These, so called, axis limits for a form factor scale of $\Lambda = 2 \text{ TeV}$ are $-1.0 < \Delta\kappa < 1.3$ ($\lambda = 0$), $-0.9 < \lambda < 0.9$ ($\Delta\kappa = 0$) for the CDF analysis, under the assumption that $\lambda_\gamma = \lambda_Z$ and $\Delta\kappa_\gamma = \Delta\kappa_Z$.

B. WW and WZ Production

Searches for particle production requiring two leptons in the final state always suffer in rate because of the small leptonic

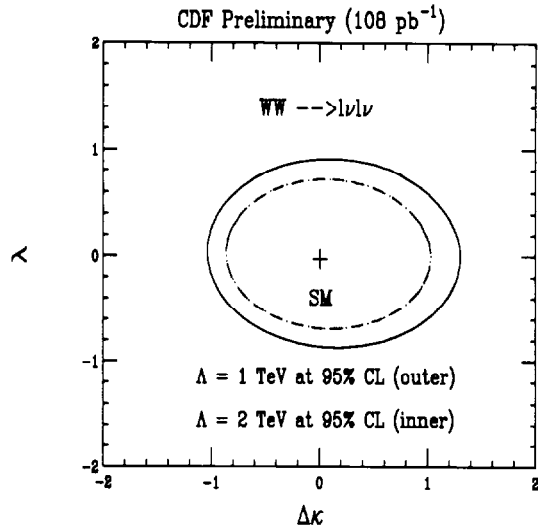


Figure 15: CDF exclusion contours in $\Delta\kappa$ and λ obtained from the measurement of the W -pair production cross section in the di-lepton channel for two different form factor scales, assuming $\lambda_\gamma = \lambda_Z$ and $\Delta\kappa_\gamma = \Delta\kappa_Z$.

branching ratios. When in the analysis described in the previous subsection only one lepton is required, a substantial increase in event rate is obtained though at the cost of a much larger background. The background from W/Z +jet production to these processes is about 30 times higher than for the signal production. Given the distinct characteristics of anomalous couplings, this background can be dealt with. Anomalous couplings modify the differential distributions dramatically, especially the transverse momentum distribution of the W -boson. The ratio $\frac{\sigma_{WW}(p_T^W=200 \text{ GeV}/c)}{\sigma_{WW}(p_T^W=20 \text{ GeV}/c)}$ is about 10^{-3} , whereas for only modest deviations from SM couplings ($\Delta\kappa = 0$, $\lambda = 1.0$) this ratio is about 0.5. By requiring the vector boson to have high transverse momentum the background is completely eliminated and a good sensitivity to anomalous couplings is retained. One completely loses sensitivity, however, to SM WW/WZ -production.

Both CDF and DØ have looked for WW and WZ -production using hadronic decay channels [40, 41]. The CDF analysis proceeds by selecting events with one high p_T lepton, large E_T and 2 jets with $E_T > 30$ GeV. Since the jets come from the hadronic decay of the gauge boson, their invariant mass is required to be consistent with the gauge boson mass, $60 < m_{jj} < 110 \text{ GeV}/c^2$. Since no distinction can be made between WW and WZ -production in this selection, the sensitivity of the study was increased by including $\bar{p}p \rightarrow WZ \rightarrow q\bar{q}\ell\ell$ events, requiring the di-lepton invariant mass to reconstruct to the Z -boson mass. In the data sample, corresponding to a total integrated luminosity of 110 pb^{-1} , no events are observed with $p_T^{jj} > 200 \text{ GeV}/c$ in the search region $60 < m_{jj} < 110 \text{ GeV}/c^2$. A background of 0.8 events from W/Z +jet events is expected and 0.1 events are predicted from SM processes. Limits on anomalous couplings

can then be set based on the event rate yielding, for $\Lambda = 2 \text{ TeV}$,

$$\begin{aligned} -0.5 < \Delta\kappa < 0.6 & \quad (\lambda = 0) \\ -0.4 < \lambda < 0.3 & \quad (\Delta\kappa = 0) \end{aligned} .$$

The DØ experiment has performed a similar analysis based on their Run 1a data sample of 14 pb^{-1} , using only $W \rightarrow e\nu$ decays. The leptonic decays of the Z are not considered in this analysis. Since gauge bosons produced from anomalous self-interactions tend to have high p_T , the jets from such a high p_T W or Z boson may not be well separated in space. In order to maximize the detection efficiency of W and Z bosons with high p_T , a small jet cone size of $\Delta R = 0.3$ was used in this analysis. The detection efficiency for hadronic decays of W and Z bosons was estimated as a function of p_T using Monte Carlo. The detection efficiency was found to be $\sim 60\%$, approximately constant up to $p_T^{jj} = 350 \text{ GeV}/c$. Differences in the estimated efficiencies from different Monte Carlo generators were included in the systematic uncertainty. The $p_T^{e\nu}$ spectrum of the final event sample of 84 events is of course dominated by background. The total number of background events was estimated to be 75.5 ± 13.3 , with 12.2 ± 2.6 events coming from QCD multi-jet events and 62.2 ± 13.0 from W +jet events. The remaining small background is mainly due to $t\bar{t}$ production. The SM prediction for WW/WZ production was 3.2 ± 0.6 events.

Because anomalous couplings not only affect the event rate but also significantly alter differential distributions, better limits on anomalous couplings are obtained when utilizing the full spectrum. DØ has performed a maximum likelihood fit to the $p_T^{e\nu}$ spectrum and, assuming equal WWZ and $WW\gamma$ couplings, obtained the following limits at 95% confidence level:

$$\begin{aligned} -0.9 < \Delta\kappa < 1.1 & \quad (\lambda = 0) \\ -0.6 < \lambda < 0.7 & \quad (\Delta\kappa = 0) \end{aligned} ,$$

using $\Lambda = 1.5 \text{ TeV}$. Comparing these limits to those obtained by CDF for the same process, but with five times the statistics using both electron and muon decays, shows the additional constraint that can be obtained from the shape of the distribution.

Since this analysis probes both $WW\gamma$ and WWZ couplings, information can be obtained on the WWZ coupling alone by setting the $WW\gamma$ couplings to their SM values. Fig. 16a shows the contour limits when SM $WW\gamma$ couplings are assumed, whereas the WWZ coupling was set to its SM value in Fig. 16b. The contours indicate that the analysis is more sensitive to the WWZ coupling than the $WW\gamma$ coupling as expected from the larger coupling strength of the WWZ vertex. Also noteworthy is the observation that the data confirms the existence of the WWZ vertex.

C. $W\gamma$ Production

The study of the production of photons in association with a W also permits a study of the $WW\gamma$ -vertex [42, 43, 44]. Most photons produced in association with a W , however, are radiated off the initial or final state fermion. The only channel that allows for a direct probe of the triple gauge boson vertex is the s -channel contribution of a photon radiated from a W . In the analyses $W\gamma$ events are selected by requiring, in addition to the

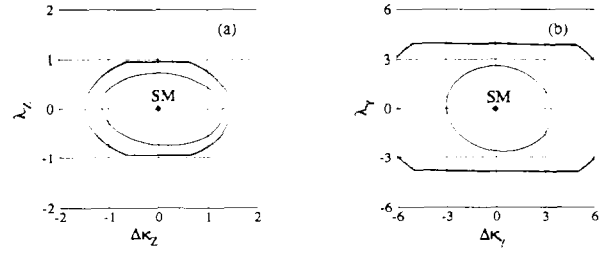


Figure 16: Contour limits on anomalous coupling parameters at the 95% CL (inner curves) and unitarity contours (outer curves) for DØ assuming $\Lambda = 1.5 \text{ TeV}$ for the process $WW/WZ \rightarrow e\nu jj$. SM couplings have been assumed for (a) $WW\gamma$ and (b) WWZ vertex.

regular W selection criteria, an isolated photon with transverse energy $E_T^\gamma > 10$ (7) GeV for DØ (CDF). Photons are detected in the pseudo-rapidity range $|\eta_\gamma| < 1.1$ for CDF and $|\eta_\gamma| < 1.1$ or $1.5 < |\eta_\gamma| < 2.5$ for DØ. The photon identification efficiencies are approximately 80% for CDF and 75% (58%) for DØ for the central (end) region. To reduce the contribution from radiative events the photon is required to be well separated from the lepton from the W -decay, $\Delta R(\ell\gamma) > 0.7$.

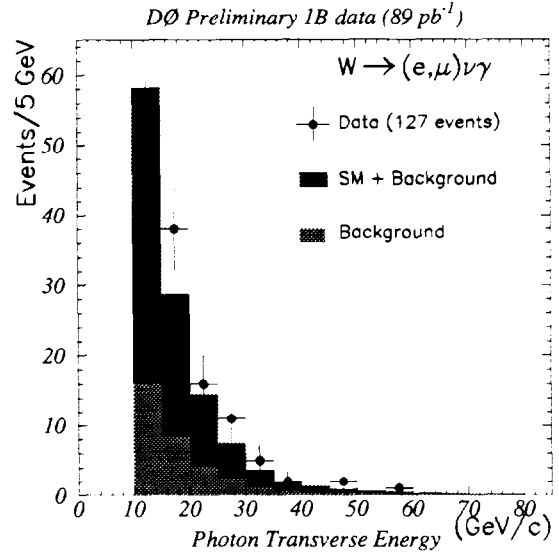


Figure 17: p_T^γ distribution of DØ $W\gamma$ candidate events.

The number of signal events, after background subtraction, and the number of expected events from SM processes are listed in table V for the electron and muon channels separately. Figure 17 shows the distribution of the photon p_T -spectrum for DØ, together with the SM expectation. Good agreement with the prediction is observed and limits could be set based on the event rate. As seen in the previous section, if the event statistics allows it, better limits on anomalous couplings are obtained by performing a maximum likelihood fit to a differential distribution. For $W\gamma$ production a binned maximum likelihood fit is performed

	DØ 87 pb ⁻¹		CDF 67 pb ⁻¹	
	$W\gamma \rightarrow e\nu\gamma$	$W\gamma \rightarrow \mu\nu\gamma$	$W\gamma \rightarrow e\nu\gamma$	$W\gamma \rightarrow \mu\nu\gamma$
N_{data}	57	70	75	34
N_{bkg}	15.2 ± 2.5	27.4 ± 4.7	16.1 ± 2.4	10.3 ± 1.2
N_{sig}	$41.8^{+8.8}_{-7.5}$	$42.6^{+9.7}_{-8.3}$	$58.9 \pm 9.0 \pm 2.6$	$23.7 \pm 5.9 \pm 1.1$
N_{SM}	43.6 ± 3.1	38.2 ± 2.8	53.5 ± 6.8	21.8 ± 4.3

Table V: Number of $W\gamma$ events observed in the data, expected background and signal events. Also listed is the number of expected events for SM couplings.

to the E_T^γ -spectrum as function of the coupling constants. The last data bin is explicitly taken to be a zero-event bin. The limits thus obtained for a form-factor scale $\Lambda = 1.5$ TeV are

$$\begin{aligned}
-1.0 < \Delta\kappa < 1.0 & \quad (\lambda = 0) & \quad (\text{DØ}) \\
-1.8 < \Delta\kappa < 2.0 & \quad (\lambda = 0) & \quad (\text{CDF}) \\
-0.3 < \lambda < 0.3 & \quad (\Delta\kappa = 0) & \quad (\text{DØ}) \\
-0.7 < \lambda < 0.6 & \quad (\Delta\kappa = 0) & \quad (\text{CDF}).
\end{aligned}$$

The corresponding contours in magnetic dipole and electric quadrupole moment, in units of the SM prediction for the moments, are shown in Fig. 18. A vanishing magnetic dipole moment and electric quadrupole moment of the W , corresponding to $\kappa = -\frac{1}{2}$ and $\lambda = -\frac{1}{2}$ is excluded at 99% CL.

The decay rate for $b \rightarrow s\gamma$ can also be used to set limits on anomalous couplings since the process is sensitive to photon radiation off the W -boson in the penguin diagram. The branching ratio has been measured by CLEO to be $B(b \rightarrow s\gamma) = (2.32 \pm 0.57 \pm 0.35) 10^{-4}$ [45]. The upper limit on this branching ratio excludes the outer regions in Fig. 18. The narrow region between the two allowed CLEO bands is excluded by the lower limit.

D. Combined Result on $WW\gamma$ Coupling

The studies of $W\gamma$ and WW/WZ production are both sensitive to the same $WW\gamma$ coupling. The analyses can thus be combined to improve on the limits on anomalous couplings. When combining results, the correlation between the different analyses needs to be addressed. Some of the dominant common systematic uncertainties are due to the method of estimating the background and the uncertainty in structure functions and photon identification. The DØ experiment has carried out a combined fit to the three data sets corresponding to the WW , WW/WZ and $W\gamma$ analyses from Run 1a. The significantly improved limits are:

$$\begin{aligned}
-0.7 < \Delta\kappa < -0.9 & \quad (\lambda = 0) \\
-0.4 < \lambda < 0.4 & \quad (\Delta\kappa = 0),
\end{aligned}$$

where it was assumed that the WWZ couplings and the $WW\gamma$ couplings were equal. Note that this combined result is more stringent than the result from the DØ $W\gamma$ analysis using the complete Run 1 data sample, showing the reach when all Tevatron results are combined.

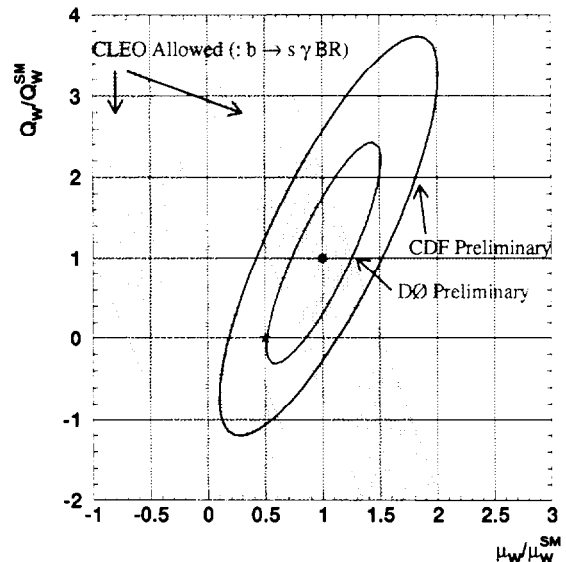


Figure 18: Limits on anomalous magnetic dipole and electric quadrupole moments for the W boson from CDF, DØ and CLEO.

E. $Z\gamma$ Production

The $ZZ\gamma$ and $Z\gamma\gamma$ trilinear gauge boson couplings are described in a way analogous to the WWV couplings. These couplings, absent in the SM, are suggested by some theoretical models which imply new physics [46]. The most general Lorentz and gauge invariant $ZV\gamma$ vertex is described by eight coupling parameters, h_i^V , ($i = 1\dots 4$), where $V = Z, \gamma$ [47]. Combinations of the \mathcal{CP} -conserving (\mathcal{CP} -violating) parameters h_3^V and h_4^V (h_1^V and h_2^V) correspond to the electric (magnetic) dipole and magnetic (electric) quadrupole transition moments of the $ZV\gamma$ vertex. Partial wave unitarity of the general $f\bar{f} \rightarrow Z\gamma$ process restricts the $ZV\gamma$ couplings uniquely to their vanishing SM values at asymptotically high energies [48]. Therefore, the coupling parameters have to be modified by form-factors $h_i^V = h_{i0}^V / (1 + \hat{s}/\Lambda^2)^n$, where \hat{s} is the square of the invariant mass of the $Z\gamma$ system and Λ is the form-factor scale. The energy dependence of the form factor is assumed to be $n = 3$ for $h_{1,3}^V$ and $n = 4$ for $h_{2,4}^V$ [49]. Such a choice yields the same

	DØ	CDF	
	89 pb ⁻¹	67 pb ⁻¹	
	<i>e</i>	<i>e</i>	<i>μ</i>
<i>N</i> _{data}	14	18	13
<i>N</i> _{bkg}	1.6 ± 0.5	0.9 ± 0.3	0.5 ± 0.1
<i>N</i> _{Sig}	12.4 ^{+4.8} _{-3.7} ± 0.5	17.1 ± 5.7	12.5 ± 3.6
<i>N</i> _{SM}	12.0 ± 1.2	16.2 ± 1.8	8.7 ± 0.7

Table VI: Number of $Z\gamma$ events observed in the data, expected background and signal events. Also listed is the number of expected events for SM couplings.

asymptotic energy behavior for all the couplings.

The study of anomalous couplings in the process $Z\gamma \rightarrow \ell\ell\gamma$ follows the same lines as the $W\gamma$ analysis [50, 51]. Table VI lists the expected and observed number of signal events for both experiments. The total cross section is seen to be in good agreement with the SM prediction. The sensitivity to anomalous couplings lies in the high p_T^γ region. Three events with $p_T^\gamma > 60$ GeV/c are observed, one by CDF and two by DØ. For DØ, the probability to observe at least two events with $p_T^\gamma > 60$ GeV/c, given a total of 14 events observed, is 8.2% and the events are consistent with a signal or background fluctuation within two standard deviations. Because of these high p_T events, however, small non-vanishing anomalous couplings are preferred in the DØ analysis. Their resulting exclusion contour from the Run 1b electron data is therefore slightly distorted (see Fig. 19). Preliminary limits on anomalous couplings for a scale factor $\Lambda = 500$ GeV from the di-electron analysis by DØ and the di-lepton analysis by CDF are, at 95% CL,

$$\begin{aligned}
-1.8 < h_{30}^Z < 1.8 & \quad (h_{40}^Z = 0) & \quad (\text{DØ}) \\
-1.6 < h_{30}^Z < 1.6 & \quad (h_{40}^Z = 0) & \quad (\text{CDF}) \\
-0.4 < h_{40}^Z < 0.4 & \quad (h_{30}^Z = 0) & \quad (\text{DØ}) \\
-0.4 < h_{40}^Z < 0.4 & \quad (h_{30}^Z = 0) & \quad (\text{CDF})
\end{aligned}$$

The DØ experiment has recently performed a new analysis looking for the decay $Z\gamma \rightarrow \nu\nu\gamma$. This channel has previously been studied only in e^+e^- -collisions [52]. Sensitivity to anomalous couplings in this channel is much higher than in the di-lepton decay modes due to the higher decay rate into neutrinos and the absence of radiative Z decay background. The overall background, however, is still extremely high, leading to very stringent event selection criteria. To reduce the background from W +jet events with the electron or jet being misidentified as a photon the E_T^γ and E_T were required to exceed 40 GeV. In addition, events with at least one jet with $E_T^j > 15$ GeV were rejected. The remaining background was dominated by cosmic rays and muons from beam halo which radiated in the calorimeter. This background was suppressed by rejecting events with a reconstructed muon or a minimum ionizing trace in the calorimeter close to the photon cluster. The residual background, which had roughly equal contributions from $W \rightarrow e\nu$ decays and muon bremsstrahlung, was derived from data.

Four candidate events are observed on an expected background of 6.4 ± 1.1 events and a SM prediction of 1.8 ± 0.2

events. Although the signal-to-background ratio is less than one, the sensitivity to anomalous couplings is still high, since the background is concentrated at low E_T^γ while the anomalous coupling contribution is almost flat in E_T^γ up to the kinematic threshold of the reaction. Limits on anomalous couplings were set at 95% CL by a fit to the E_T^γ spectrum and gives $|h_{30}^Z| < 0.9$, $|h_{40}^Z| < 0.2$. This represents a factor of two improvement compared to the combined DØ Run 1a limits from the di-lepton analysis, based on the same luminosity [51]. A summary of all the limits is shown in Fig. 19 [50, 51, 52]. The L3 contour has a different orientation because of the different subprocess center of mass energy at which the events are produced.

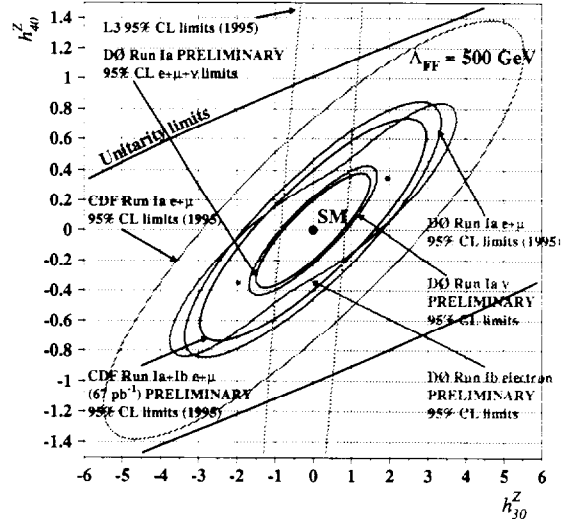


Figure 19: Limits on anomalous CP -conserving $ZZ\gamma$ couplings from $Z(\ell\ell)\gamma$ and $Z(\nu\nu)\gamma$ production. The dashed line is the unitarity contour for a form-factor scale $\Lambda = 500$ GeV.

IX. CONCLUSIONS

A wide variety of properties of the W and Z -bosons are now being studied at hadron colliders with ever increasing precision, at the highest energy scales achievable. All results, including the results from e^+e^- colliders [53, 54], are in good agreement with the SM. It is widely anticipated, though, that the SM is just an approximate theory and should eventually be replaced by a more complete and fundamental description of the underlying forces in nature. With the new data from LEP 2, SLD and the Tevatron, and with the planned upgrades of the accelerators as well as the experiments, the projected uncertainties [55] on some fundamental parameters should provide the tools to take another ever more critical look at the SM, without any theoretical prejudice.

X. ACKNOWLEDGEMENTS

I would like to thank Debbie Errede, Paul Grannis, Young-Kee Kim and Darien Wood who have been very helpful.

XI. REFERENCES

- [1] S. Abachi *et al.* (DØ Collaboration), Nucl. Instr. Meth. **A338**, 185 (1994); H. Aihara *et al.* (DØ Collaboration), Nucl. Instr. Meth. **A325**, 393 (1993); S. Abachi *et al.* (DØ Collaboration), Nucl. Instr. Meth. **A324**, 53 (1993).
- [2] F. Abe, *et al.* (CDF Collaboration), Nucl. Instr. Meth. **A271**, 387 (1988).
- [3] F. Abe, *et al.* (CDF Collaboration), Phys. Rev. Lett. **73**, 220 (1994); F. Abe *et al.*, Phys. Rev. **D52**, 2624 (1995).
- [4] W. F. Badgett, "Proceedings of the 8th DPF Meeting", August 2-6 (1994), 431, Albuquerque, New Mexico
F. Abe, *et al.* (CDF Collaboration), FERMILAB-PUB-95-301-E (1995) (submitted to Phys. Rev. Lett.)
- [5] S. Abachi *et al.* (DØ Collaboration), Phys. Rev. Lett. **75**, 1456 (1995)
- [6] R. Hamberg, W. L. van Neerven and T. Matsuura, Nucl. Phys. **B359**, 343 (1991); W. L. van Neerven and E. B. Zijlstra, Nucl. Phys. **B382**, 11 (1992).
- [7] Although these mass values have been updated recently [53], these are the averages used for the published results.
- [8] H. L. Lai *et al.*, Phys. Rev. **D51**, 4763 (1995).
- [9] J. L. Rosner, M. P. Worah and T. Takeuchi, Phys. Rev. **D49**, 1363 (1994).
- [10] Particle Data Group, R.M. Barnett *et al.*, Phys. Rev. D **54**, 1 (1996).
- [11] C. Albajar *et al.* (UA1 Collaboration), Phys. Lett. **B253**, 503 (1991).
- [12] J. Alitti *et al.* (UA2 Collaboration), Phys. Lett. **B276**, 365 (1992).
- [13] F. Abe *et al.* (CDF Collaboration), Phys. Rev. Lett. **74**, 341 (1995).
- [14] E. Eichten, K. Lane, M. Peskin Phys. Rev. Lett. **50** (1983) 811.
- [15] F. Abe *et al.* (CDF Collaboration), Phys. Rev. Lett. **67**, 2418 (1991); F. Abe *et al.*, Phys. Rev. D **49**, 1 (1994)
- [16] The angle ϑ is the polar angle of the outgoing fermion with respect to the incoming proton beam. Pseudorapidity is defined as $\eta = -\ln \tan \frac{\vartheta}{2}$. An asterisk indicates quantities in the parton center of mass frame.
- [17] F. Abe *et al.* (CDF Collaboration), Phys. Rev. Lett. **77**, 2616 (1996).
- [18] A. D. Martin, R. G. Roberts and W. J. Stirling, Phys. Lett. **B306**, 145 (1993); **B309**, 492(E) (1993);
A. D. Martin, R. G. Roberts and W. J. Stirling, Phys. Rev. **D50**, 6734 (1994)
- [19] J. Rosner, Phys. Rev. D **54**, 1078 (1996).
- [20] For alternate methods see the contributions by S. Keller and S. Rajagopalan, *these proceedings*
- [21] F. Abe *et al.* (CDF Collaboration), Phys. Rev. Lett. **75**, 11 (1995);
F. Abe *et al.* Phys. Rev. **D52**, 4784 (1995).
- [22] S. Abachi *et al.* (DØ Collaboration), Phys. Rev. Lett. **77**, 3309 (1996); M.L. Kelly *et al.* Fermilab-Conf-96/236.
- [23] The reference mass values used are $M_Z^{LBP} = 91.1884 \pm 0.0022 \text{ GeV}/c^2$, $M_{J/\psi} = 3.09688 \pm 0.00004 \text{ GeV}/c^2$ and $M_{\psi^0} = 0.1350 \pm 0.0006 \text{ GeV}/c^2$, Particle Data Group, L. Montanet *et al.*, Phys. Rev. D **50**, 1173 (1994).
- [24] G. Ladinsky and C.-P. Yuan, Phys. Rev. D **50**, 4239 (1994).
- [25] F. Abe *et al.* (CDF Collaboration), Phys. Rev. Lett. **74**, 850 (1995)
- [26] M. Demarteau *et al.*, Combining W Mass Measurements, CDF/PHYS/CDF/PUBLIC/2552 and DØ NOTE 2115.
- [27] J. Alitti *et al.* (UA2 Collaboration), Phys. Lett. **B276**, 354 (1992);
F. Abe *et al.* (CDF Collaboration), Phys. Rev. Lett. **65**, 2243 (1990), Phys. Rev. D **43**, 2070 (1991);
- [28] CCFR Collaboration (C. Arroyo, B.J. King *et al.*) Phys. Rev. Lett. **72**, 3452 (1994); K. McFarland in "Proceedings of the XXXI Rencontres de Moriond, Electroweak Interactions and Unified Theories, 16-23 March, 1996, Les Arcs, Bourg Saint Maurice, France (ed. Jean Trân Thanh Vân), Fermilab-Conf-96/227
- [29] A. Bodek (CDF Collaboration) FERMILAB-CONF-96/381-E, to appear in "Proceedings of the Cracow International Symposium on Radiative Corrections (CRAD96)", Cracow, Poland, August 1-5, 1996.
- [30] CDF's "Aha Erlebnis".
- [31] W. Giele, E. Glover, D. A. Kosower, Nucl. Phys. **B403**, 663 (1993).
- [32] M. Glück, E. Reya, A. Vogt Z. Phys. **C67**, 433 (1995).
- [33] F. Abe *et al.* (CDF Collaboration), Phys. Rev. Lett. **69**, 2160 (1992)
- [34] J. Alitti *et al.* (UA2 Collaboration), Phys. Lett. **B277**, 203 (1992).
- [35] F. Abe *et al.* (CDF Collaboration), Phys. Rev. Lett. **76**, 2852 (1996).
- [36] L. Amellos, W.J. Marciano and Z. Parsa, Nucl. Phys. **B196**, 378 (1982).
- [37] K. Kim and Y-S. Tsai, Phys. Rev. D **7**, 3710 (1973).
- [38] U. Baur and E.L. Berger, Phys. Rev. D **41**, 1476 (1990).
- [39] S. Abachi *et al.* (DØ Collaboration), Phys. Rev. Lett. **75**, 1023 (1995)
- [40] F. Abe *et al.* (CDF Collaboration), Phys. Rev. Lett. **75**, 1017 (1995)
- [41] S. Abachi *et al.*, Phys. Rev. Lett. **77**, 3303 (1996).
- [42] J. Alitti *et al.*, Phys. Lett. **B277**, 194 (1992).
- [43] F. Abe *et al.* (CDF Collaboration), Phys. Rev. Lett. **74**, 1936 (1995)
- [44] S. Abachi *et al.* (DØ Collaboration), Phys. Rev. Lett. **75**, 1034 (1995).
- [45] M.S. Alam *et al.* (CLEO Collaboration), Phys. Rev. Lett. **74**, 2885 (1995) 2885.
- [46] H. Aihara *et al.*, in "Electroweak Symmetry Breaking and Beyond the Standard Model", report from the DPF Long-Range Planning Study, eds. T. Barklow, S. Dawson, H. Haber and J. Siegrist.
- [47] K. Hagiwara *et al.*, Nucl. Phys. **B282**, 253 (1987).
- [48] K. Hagiwara and D. Zeppenfeld, Nucl. Phys. **B274**, 1 (1986);
U. Baur and D. Zeppenfeld, Phys. Lett. **201B**, 383 (1988).
- [49] U. Baur and E.L. Berger, Phys. Rev. **D47**, 4889 (1993).
- [50] F. Abe *et al.* (CDF Collaboration), Phys. Rev. Lett. **74**, 1941 (1995)
- [51] S. Abachi *et al.* (DØ Collaboration), Phys. Rev. Lett. **75**, 1028 (1995)
- [52] M. Acciarri *et al.* (L3 Collaboration), Phys. Lett. **B346**, 190 (1995).

- [53] M. Demarteau, Fermilab-Conf-96/354, to appear in the "Proceedings of the Meeting of the Division of Particles and Fields", Minneapolis, MN, August 10 – 15, 1996.
- [54] M. Swartz, *these proceedings*.
- [55] See, for example, U. Baur, M. Demarteau, *these proceedings*.